

# Intelligent Spatial Interpolation-based Frost Prediction Methodology using Artificial Neural Networks with Limited Local Data.

Ian Zhou, *Graduate Student Member, IEEE*, Justin Lipman, *Senior Member, IEEE*,  
Mehran Abolhasan, *Senior Member, IEEE*, and Negin Shariati, *Member, IEEE*

**Abstract**—The weather phenomenon of frost poses great threats to agriculture. Since it damages the crops and plants from upstream of the supply chain, the potential impact of frosts is significant for agriculture-related industries. As recent frost prediction methods are based on on-site historical data and sensors, extra development and deployment time are required for data collection in any new site. The aim of this article is to eliminate the dependency on on-site historical data and sensors for frost prediction methods. In this article, a frost prediction method based on spatial interpolation is proposed. The models use climate data from existing weather stations, digital elevation models surveys, and normalized difference vegetation index data to estimate a target site’s next hour minimum temperature. The proposed method utilizes ensemble learning to increase the model accuracy. Ensemble methods include averaging and weighted averaging. Climate datasets are obtained from 75 weather stations across New South Wales and Australian Capital Territory areas of Australia. The models are constructed with five-fold validation, splitting the weather stations into five testing dataset folds. For each fold, the other stations act as training datasets. After the models are constructed, three experiments are conducted. The first experiment compares the results generated by models between different folds. Then, the second experiment compares the accuracy of different methods. The final experiment reveals the effect of available stations on the proposed models. The results show that the proposed method reached a detection rate up to 92.55%. This method could be implemented as an alternative solution when on-site historical datasets are scarce.

**Index Terms**—Frost Prediction, Internet of Things, Machine Learning, Spatial Interpolation, Spatial Prediction.

## I. INTRODUCTION

Frost is a devastating weather phenomenon that could induce critical losses to agriculture-related industries [1]. As frost events are capable of eliminating the crops from the upstream of supply chains, it could affect jobs and businesses along the entire supply chain [2]. Fortunately, frost events could be predicted and detected. Recent frost prediction methods are based on machine learning models [3]. These models require historical data from a specific site to predict future frost events. However, this requirement of on-site historical data poses a restriction for model construction in new sites without historical data [3]. Long periods of time are needed for data collection at these new sites to construct and deploy the machine learning models. After the models are constructed, local sensor nodes are needed to feed live data to the prediction models. This is another restriction of recent methods. To overcome these restrictions, this article proposes a frost prediction method based on spatial interpolation techniques, aiming to

predict frost for a site without any on-site historical data or sensors.

Spatial interpolation includes methods that generate or predict spatially continuous data from a few regional sample points [4]. The authors of [5] compared different spatial interpolation methods for monthly air temperatures at Mt. Kilimanjaro, Tanzania. They found that model averaging neural networks and Artificial Neural Networks (ANNs) are ranked fourth and fifth in accuracy, respectively. ANNs are also the most accurate model type within recent frost prediction techniques. Therefore, in this article, the proposed method uses ANN as the base model and baseline.

The proposed method is an ensemble learning method that utilizes the existing historical data from 75 weather stations across New South Wales (NSW) and Australian Capital Territory (ACT) in Australia. Several weak predictors are trained. Each of the weak predictors is created using the climate features from one specific station to predict the next hour minimum temperatures of other weather stations. Location features from both stations are also included. The location features include geographical location, elevation from the Digital Elevation Model (DEM), and Normalized Difference Vegetation Index (NDVI), indicating the amount of green vegetation [6]. These location features are also used to aggregate the results of the weak predictors.

### A. Related Work

Recent frost prediction methods can be divided into “classification methods” and “regression methods” [3]. The classification methods predict the probability of frost occurrence in the future. The regression methods predict the future minimum temperature. As different crops have different resistance to frost [7], this article focuses on regression methods of frost prediction. Along with the regression methods, different triggering temperatures for frost can be applied as a general solution for different types of crops and plants.

The majority of recent frost prediction regression methods [8], [9], [10], [11], [12], [13] predict the minimum temperature of the next 12–24 hours. The prediction models include, linear regression [8], [9], random forest [10], and ANNs [11], [12], [13]. The ANNs have the highest accuracy among the other model types [3].

All these methods [8], [9], [10], [11], [12], [13] depend on local/on-site historical climate data for model training, validation, testing and future operations. This first generates extra

development and deployment time to collect local climate datasets. Then, a live sensor system is required to transmit data to the prediction models. The proposed method in this article aims to remove the model dependency of on-site data and sensors. Models can be built from existing historical data from other weather stations, previously surveyed DEM, and NDVI data from satellites. During operation time, the model input sources are also climate data from other weather stations, previously surveyed DEM, and NDVI data from satellites. The proposed method does not require on-site data or sensors. The major contributions of this article are:

- 1) Proposing a spatial interpolation-based frost prediction method.
- 2) Eliminating the on-site data/sensor requirement for frost regression prediction methods.
- 3) Exploring the performance of an off-site frost prediction method.

The rest of the paper is organized as follows. Section II presents the methodology. This includes the descriptions of data sources, data preprocessing methods, model types, and experiment settings. The experiments compare the performance of the proposed method with the baseline method derived from on-site climate datasets. Then, Section III shows the experiment results along with the discussions on limitations. Finally, the paper is concluded in Section IV.

## II. METHODOLOGY

In this section, the data processing and experiment procedures are presented. To start all experiments, multiple datasets are obtained from different data sources. These datasets and their sources are described. Then, the data preprocessing steps are demonstrated, followed by the model structure of the prediction models. Finally, this section explains the experiment settings.

### A. Data Sources

The data sources can be grouped into four categories. These categories are climate data, DEM data, NDVI data and state boundary data. The climate datasets are obtained from 75 different weather stations across NSW and ACT. The raw datasets can be obtained from the Australian Bureau of Meteorology (BOM) website [14]. In the climate data category, there are two groups of datasets. The first group consists of datasets from the year 2017. These datasets are used for model training, validation, and preliminary testing. The second group is datasets from June, July, and August (winter [15]) of 2018. These datasets are used to test the model performance in the winter one year after the models are constructed.

The second data source category includes a DEM dataset of the study area. The DEM dataset contains 1 second (about 30 m) resolution elevation data of Australia. The NSW and ACT portion of the DEM dataset is extracted to be used as features during model construction, validation, and testing. The raw DEM dataset is hosted by Geoscience Australia [16].

The raw NDVI datasets are collected from the Land Processes Distributed Active Archive Center of NASA [17]. The data resolution is 250 m. Similar to the climate datasets, NDVI

datasets are from the year 2017 and the winter months of 2018. The datasets from 2017 are also used for model training, validation, and preliminary testing. The NDVI datasets from 2018 act as features during the final testing phase to evaluate the model performance in the winter one year after model construction.

Boundary datasets form the final data category in this article. There are two separate data files that contain boundary information of NSW and ACT. The area coverage is defined by coordinates of multiple polygon vertices. The boundary datasets are not directly involved in the process of model training, validation, or testing. However, the boundary datasets are required when extracting the NSW and ACT portion of the DEM and NDVI datasets. The boundary datasets of NSW and ACT can be obtained from [18] and [19], respectively.

### B. Data Preprocessing

Data preprocessing procedures are described according to the data categories defined in the above subsection. Climate data preprocessing is explained first, followed by DEM data preprocessing and NDVI data preprocessing. The boundary data is used during the preprocessing of DEM and NDVI datasets. However, as boundary data is not included in the processes of model training, validation, and testing, the usage of boundary data is only presented with other data categories. After the preprocessing of the four data categories, the datasets are merged to be fit as training data of prediction models. This merging process is also explained.

Each climate data file stores climate data from a different weather station. The temperature, dew point, Relative Humidity (RH), wind speed, and wind direction fields are extracted from each of these stations. Wind speed and direction are converted to *N-wind* and *E-wind*, as the north and east components of the wind. This conversion is done by reversing the wind direction (*met*) to the wind blowing direction (*deg*) (Equation 1) [20]. Then, calculating the magnitude of the eastward ( $v_E$ ) and northward ( $v_N$ ) wind components with the wind speed ( $v$ ) and wind blowing direction (*deg*) (Equation 2). After computing the wind components, the next hour minimum temperature is calculated as the training targets of the models. For each time step at each weather station, the target is obtained from the minimum temperature of the next 60 time steps.

$$deg = \begin{cases} met + 180^\circ, & \text{if } met < 180^\circ \\ met - 180^\circ, & \text{if } met \geq 180^\circ \end{cases} \quad (1)$$

$$v_E, v_N = v \times \sin(deg), v \times \cos(deg) \quad (2)$$

Since the spatial interpolation models are built with five-fold validation, the weather stations are randomly divided into five folds. For each model fold, one different fold of the weather stations (15 stations) is used as testing data sources and the rest of the weather stations are used as training data sources. Figure 1 shows the distribution of weather station folds. Detailed coordinates of the fold stations are recorded in Tables X and XI in Appendix C.

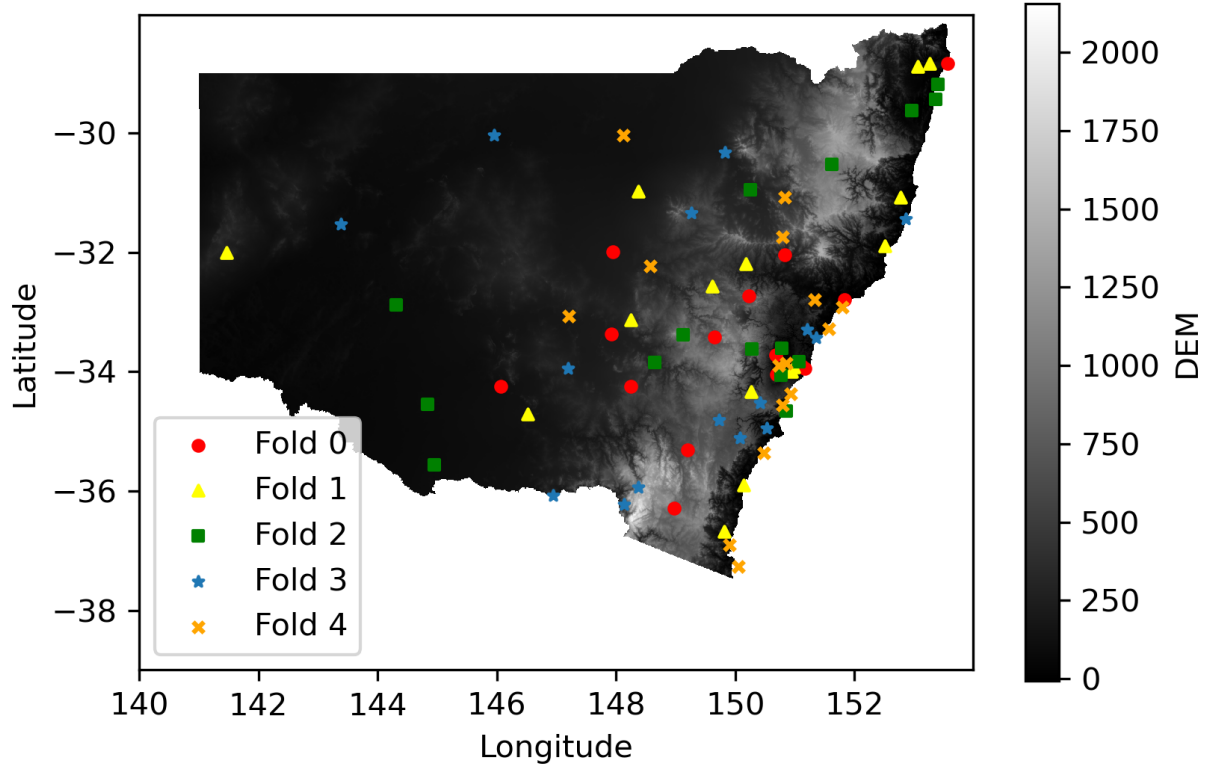


Fig. 1. Distribution of Station Folds on NSW and ACT DEM Map.

The DEM dataset is resampled to a grid with a cell size of  $0.01^\circ \times 0.01^\circ$  (approximately  $1.11 \text{ km} \times 1.11 \text{ km}$ ). Then, the NSW and ACT parts of the map are extracted according to the boundary datasets. The DEM readings of Figure 1 is the result of DEM preprocessing. The NDVI datasets are preprocessed with the same procedures as the DEM dataset. These datasets are also resampled to a  $0.01^\circ \times 0.01^\circ$  grid. Then, data is extracted within NSW and ACT boundaries.

Table I shows five features groups. The training data required by all models in this article can be represented by assembling some of the five feature groups. There are two data input formats that correspond to the two model types. The first model type is the baseline model. This model type requires on-site climate data for prediction. Therefore, the source station climate features are required as the input features of these models, and the next hour minimum temperature of the source station is used as the model target or predictand.

The second model type provides off-site frost predictions. For each model prediction, the models utilize climate data from a source station and predict the next hour minimum temperatures for a target station in another locations. The source station attributes and target station attributes are acquired as the features to compute the differences between stations (Location, DEM, NDVI). Also, the source station climate features are input as climate references. Finally, the spatial model predictand is the minimum temperature values

from the target station.

TABLE I  
FEATURES AND PREDICTANDS OF PREPROCESSED DATASETS

Feature Groups	Features
Source Station Attributes	Longitude, Latitude, DEM, NDVI
Target Station Attributes	Longitude, Latitude, DEM, NDVI
Source Station Climate Features	Temperature, Dew Point, RH, N-wind, E-wind
Baseline Predictand	Source Station Minimum Temperature
Spatial Model Predictand	Target Station Minimum Temperature

### C. Model Types

This article involves two major model types. They are the baseline models and spatial interpolation-based models. Baseline models are ANN models that harness data from sensors at a particular site and predict frost on the site. Every model is designed to predict frost for one different location. These models represent recent frost prediction models that are built from on-site historical climate datasets.

Spatial interpolation-based models are also ANN models. Unlike the baseline models, the spatial interpolation-based

models do not need on-site sensor data from the target location. These models use off-site climate data from weather stations of other locations to predict any frost of the target location. In this article, there are multiple spatial interpolation-based models. Each model in each station fold is constructed based on the climate data of a different source station, and the target stations of that model are the testing stations of the fold. To increase the accuracy of predictions, the results within a fold are aggregated. Two results aggregation methods are tested. The first method is averaging all results within each fold. The second method is to compute a weighted average based on the difference between each source station and the target location/station. This difference is calculated by geographical coordinates, DEM, and NDVI.

1) *Weighted Average Layer*: The weighted average layer is applied after obtaining the results of multiple spatial interpolation-based models in a particular fold. A weight is calculated for every station that provided a valid prediction result. An intermediate weight for the  $i$ th source station ( $W_i$ ) is first calculated by Equation 3.  $g_i$ ,  $d_i$ , and  $n_i$  are normalized geographical distance, DEM difference, and NDVI difference between the source station and the target location. The geographical distance is computed as a two-dimensional Euclidean distance. DEM and NDVI differences are one-dimensional Euclidean distances.  $a$ ,  $b$ , and  $c$  provide adjustable importance of the geological distance, DEM difference, and NDVI difference to the station weight. Currently, the adjustable weights (Table II) are generated by Pearson Correlation between each of the distance/differences and model errors. After the intermediate weights for all stations are obtained, these intermediate weight for each station is divided by the sum of the intermediate weights. The final station weights are obtained by normalizing the divided intermediate weights.

$$W_i = \frac{1}{ag_i + bd_i + cn_i} \quad (3)$$

TABLE II  
ADJUSTABLE WEIGHTS FOR DIFFERENT FOLDS

Fold Number	Geo Weight (a)	DEM Weight (b)	NDVI Weight (c)
0	0.1629	0.0132	0.0290
1	0.1768	0.0205	0.0238
2	0.1612	0.0222	0.0177
3	0.1804	0.0114	0.0269
4	0.1601	0.0110	0.0260

#### D. Experiments

To compare the results of the off-site prediction models with the baseline, three experiments are conducted. The aim of the first experiment is to compare the prediction results of different folds and determine if biasedness exists due to different station training data. Three sets of raster maps of NSW and ACT are generated from the datasets acquired in the year 2017. These raster maps are computed from the spatial interpolation-based models. Each map of the first set is created using the results

from one different weather station. The second set is created by averaging the first map set per fold. After that, the final map set is generated using the weighted average layer.

The second experiment compares the accuracy between the three model types (baseline, averaging, weighted averaging). The testing datasets are from 2017. The baseline models use parts of the datasets not involved in the training process (20% of data for each station from 2017). For spatial interpolation-based models, 15 weather stations per fold act as testing datasets (Tables X and XI).

In the final experiment, datasets from the winter months of 2018 are used to compare the spatial interpolation-based models with different numbers of available stations. Model accuracy is compared against the baseline models. After that, the percentages of captured events below zero degrees are also evaluated. An event is determined as a time step, where the temperature is below zero degrees. An event is captured when the prediction algorithm predicts that the temperature is below zero degrees at the time step of the event.

### III. RESULTS AND DISCUSSIONS

#### A. Effect of Different Fold Training Datasets

In this experiment, the differences in the results generated by models trained and tested with different datasets are revealed. As examples, one test station is randomly chosen from each of the weather station folds. For each of the stations, four raster maps generated from models trained with climate data from the station are compared from the other four folds. The five stations are stations 63297, 66137, 58212, 72160, and 67119, from folds 0, 1, 2, 3, and 4, respectively.

TABLE III  
P-VALUE MATRIX FOR COMPARING RASTER MAP RESULTS OF MODELS USING WEATHER STATION 63297 AS CLIMATE DATA SOURCE AND TRAINED WITH THE DATASETS FROM FOLDS 1–4

	Fold 1	Fold 2	Fold 3	Fold 4
Fold 1	N/A	0.00	7.87e-61	0.00
Fold 2	0.00	N/A	0.00	0.00
Fold 3	7.87e-61	0.00	N/A	0.00
Fold 4	0.00	0.00	0.00	N/A

Figure 2 shows the raster maps generated from individual models of station 63297 constructed by the training data (excluding the data from testing stations in each test fold) in fold 1–4. From a visual perspective, the raster maps of the four folds are similar in major features. For example, all maps present heat spots in the northeastern and northwestern regions. Also, all maps demonstrate the cold spot near the center of the maps. However, the shapes of these features are different between each fold. Folds 2 and 3 show more details than the other two folds. The maps seem to be significantly affected by the available training datasets for different folds. Table III also supports the hypothesis that raster map results are affected by the different training datasets in each fold. Table III is the P-value matrix by conducting paired T-tests for all possible fold raster map result pairs. All of the P-values are smaller than 0.05. This rejects the null hypothesis

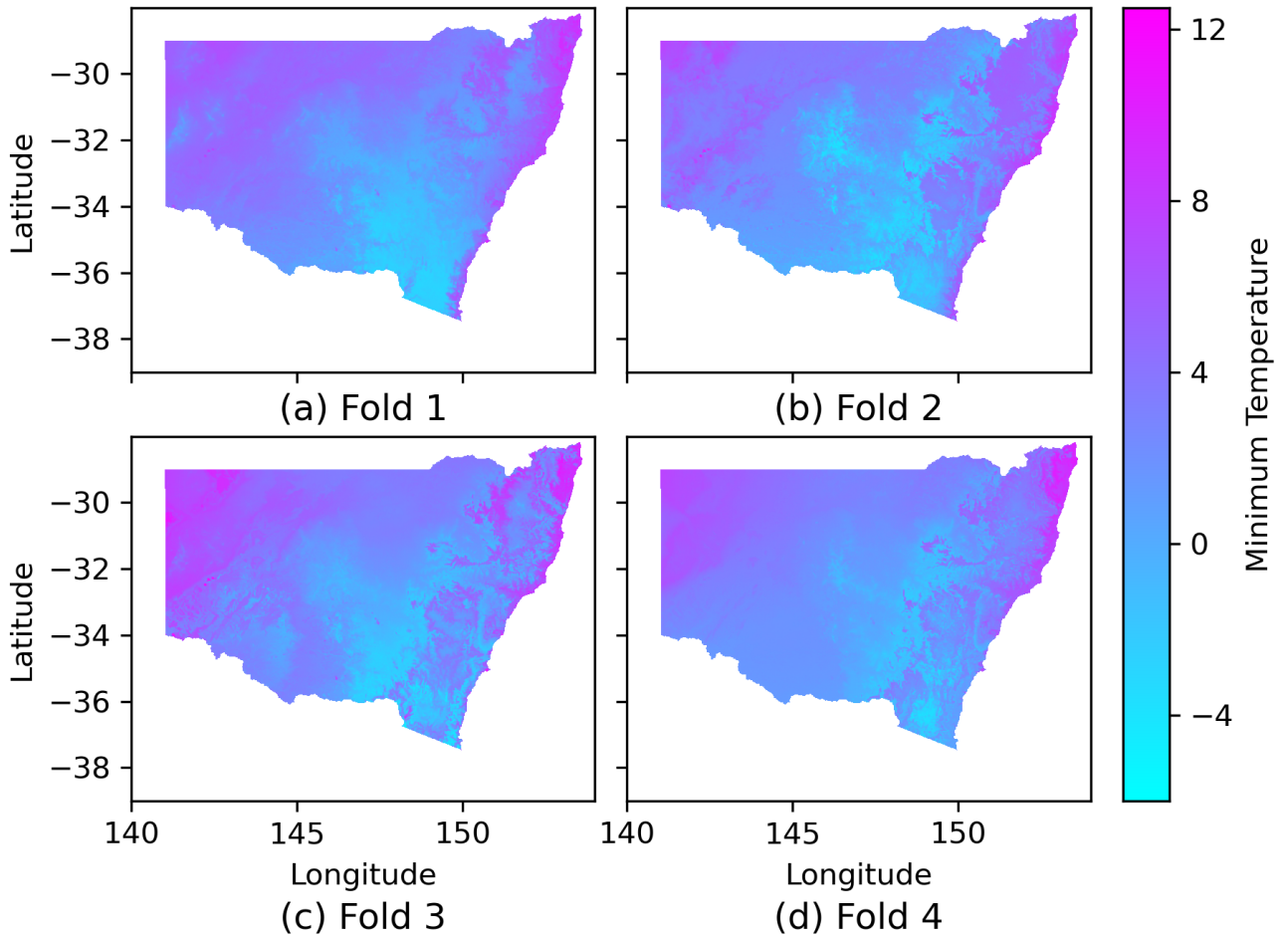


Fig. 2. Raster Maps from Models Using Weather Station 63297 as Climate Data Source Trained with the Datasets from Folds 1-4.

and favors the alternative hypothesis that the raster maps are different from each other. Raster maps from stations 66137, 58212, 72160, 67119 draw similar conclusions. The raster maps of these stations are placed in Appendix A and the P-value matrices are placed in Appendix B.

Raster maps (Figure 3) are also generated for the averaged result of each folds. Compared to the maps generated from individual models, maps of averaging models per fold are more visually similar. However, The results of paired T-tests (Table IV) are similar to the individual models. All of the P-values are smaller than 0.05. This suggests strong evidence against the null hypothesis. There are significant differences between these averaged maps from different folds. These differences also exist between weighted averaged maps.

Finally, raster maps (Figure 13 in Appendix A) created from weighted averages of models within each fold present similar properties to the averaged maps. From the T-tests (Table IX in

TABLE IV  
P-VALUE MATRIX FOR COMPARING AVERAGED RASTER MAP RESULTS OF EACH FOLD

	Fold 0	Fold 1	Fold 2	Fold 3	Fold 4
Fold 0	N/A	0.00	0.00	0.00	0.00
Fold 1	0.00	N/A	0.00	0.00	0.00
Fold 2	0.00	0.00	N/A	0.00	2.67e-121
Fold 3	0.00	0.00	0.00	N/A	0.00
Fold 4	0.00	0.00	2.67e-121	0.00	N/A

Appendix B), the effect of different training station datasets still persists.

### B. Model Accuracy

In the second experiment, model accuracy is compared between individual station models for different folds, an averaged

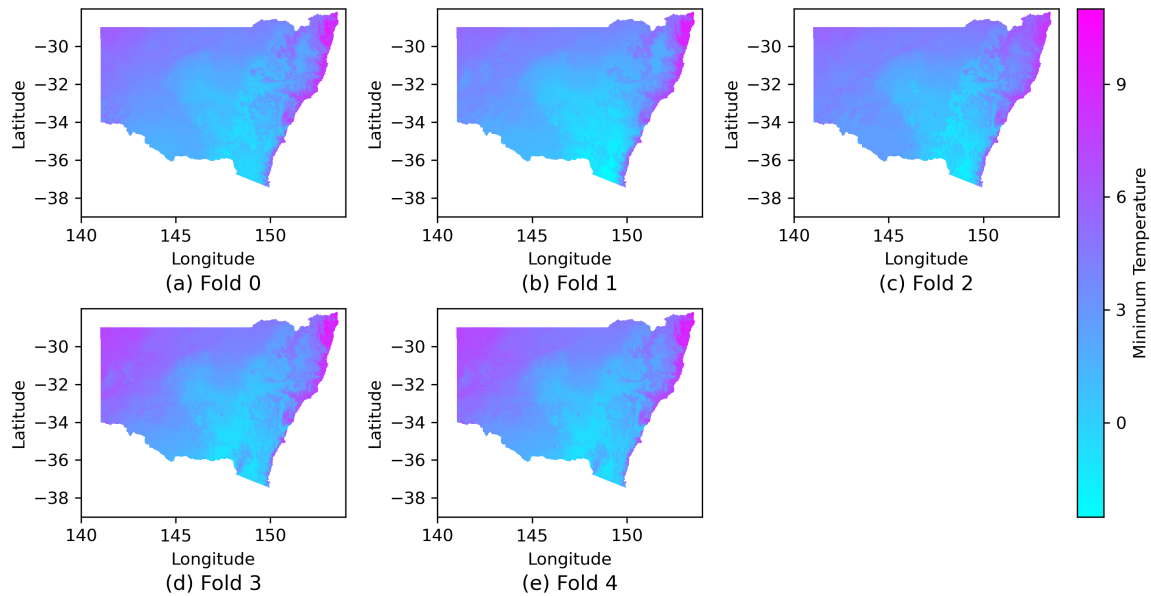


Fig. 3. Raster Maps from Averaged Results per Fold.

station result per fold, a weighted average result of station models per fold, and the baseline. The baseline, using on-site sensor data, reaches the highest accuracy with the lowest Root Mean Square Error (RMSE). The ensemble methods of averaging and weighted averaging outperform the individual station models in the spatial interpolation-based methods. Ensemble by weighted average reached higher accuracy because higher weights are given to stations that are much similar to the target locations.

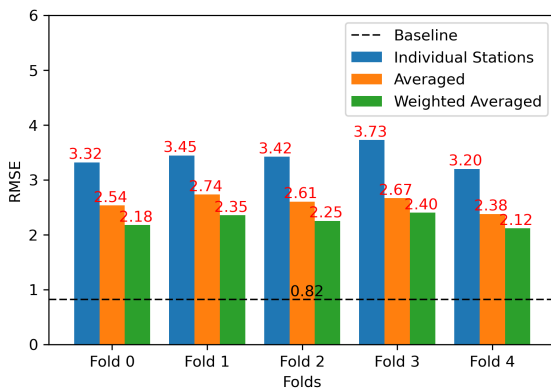


Fig. 4. RMSE of Individual, Averaged, Weighted Averaged Models Obtained from Year 2017 Testing Datasets.

### C. Effect of the Number of Available Weather Stations

In the final experiment, the ability of fault tolerance of the proposed ensemble methods is tested. The accuracy and event capture rate of the averaged and weighted averaged methods are tested with different numbers of available weather

stations. This experiment focuses more on the ability to capture potential events below zero degrees in the future. Most of the baseline models achieved 100% of event detection rate (true positive rate) in this experiment. The mean true positive rate of the baseline models is 99.62%. To ensure fairness of the experiment, the testing datasets are from the year 2018 (a year after the training datasets).

Figure 5 shows the accuracy of the proposed ensemble methods with different numbers of available weather stations 10, 20, 30, 40, 50, and 60. The weighted averaged method outperforms the averaged method with a lower RMSE. Accuracy for both methods increases as the number of stations increases.

Contrary to the accuracy, the event capture rate or true positive rate reduces as the number of stations increases (Figure 6). However, the false discovery rate also reduces with the increase of the number of available stations. This illustrates that the event detection rate is high due to high false positives. The ensemble of results with more stations reduces error. However, high errors induce lower temperature predictions, which increase the event capture rate with the number of false positives. Another experiment with the number of available stations 1–10 is conducted to inspect the relationship between true positive rate and false discovery rate.

The RMSE (Figure 7) of the ensemble methods for 1–10 stations follows previous patterns. RMSE reduces with the increase of the number of available stations. The true positive rate performs a more extreme pattern. When there is only one available station, the true positive rate could exceed 90% (Figure 8). However, the false discovery rate also exceeds 90% when there is only one available station. In conclusion, as the accuracy of temperature prediction reduces, the models recognize more events. This increase of event recognition

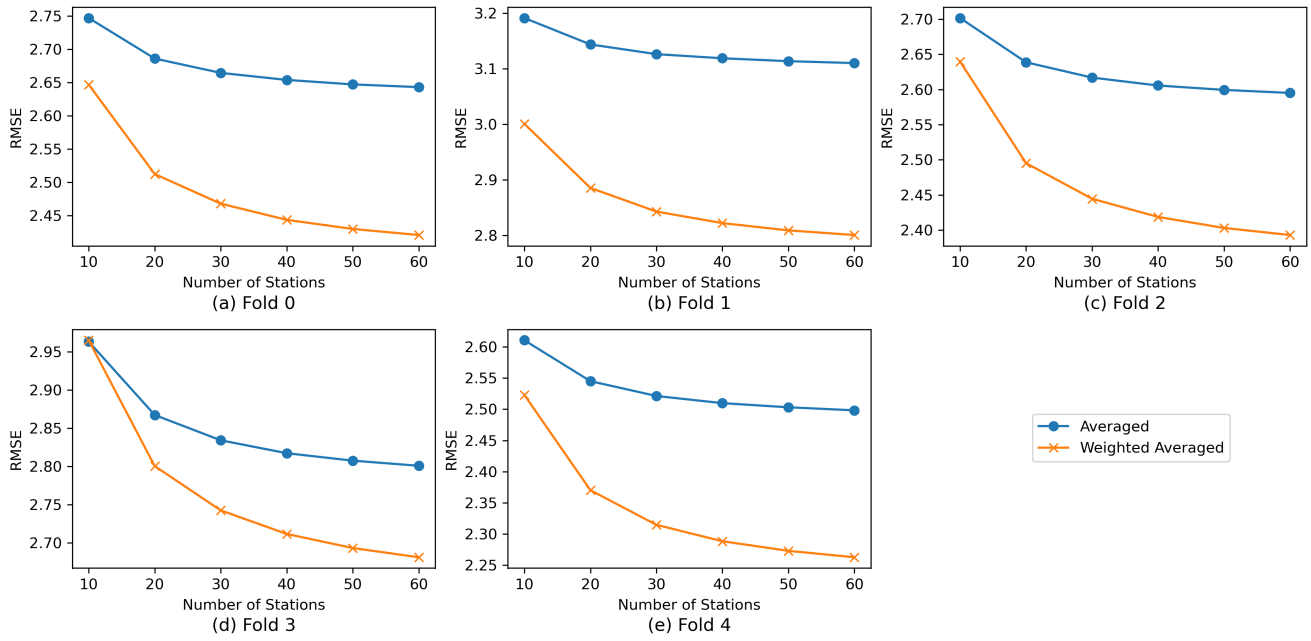


Fig. 5. RMSE of Averaged and Weighted Averaged Models with 10–60 Available Stations Obtained from Year 2018 Testing Datasets.

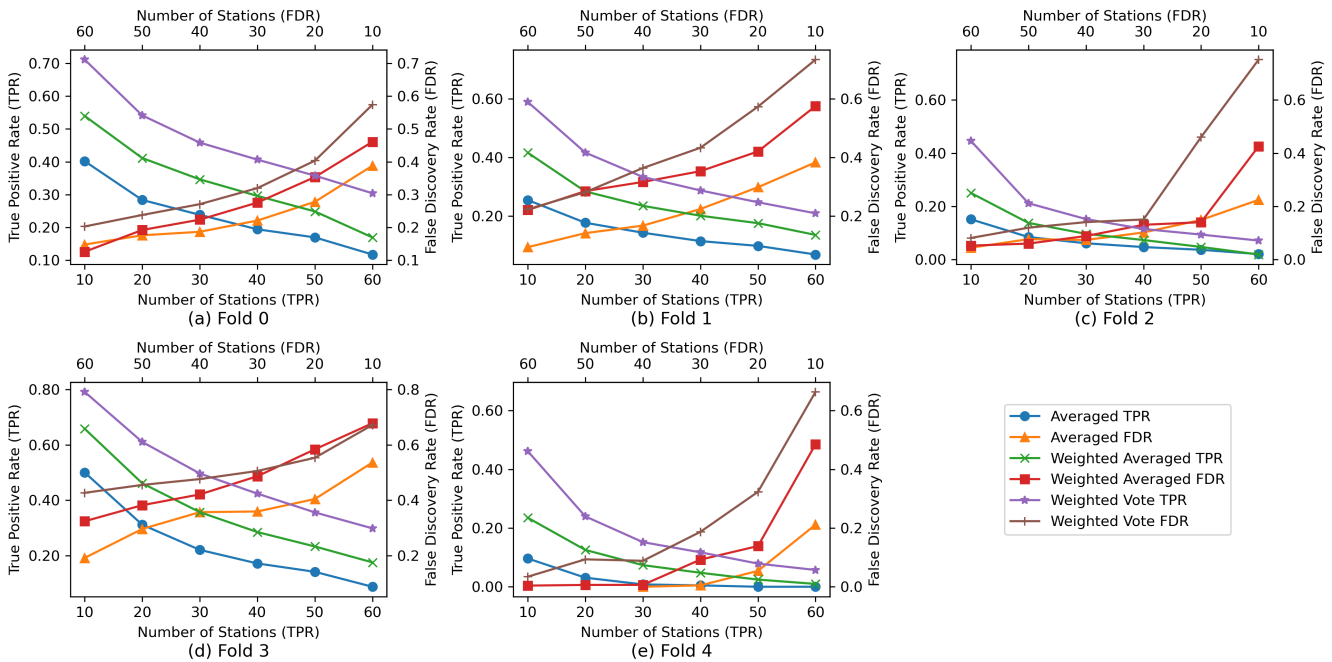


Fig. 6. True Positive Rate and False Discovery Rate of Averaged, Weighted Averaged, and Weighted Voting Models with 10–60 Available Stations Obtained from Year 2018 Testing Datasets.



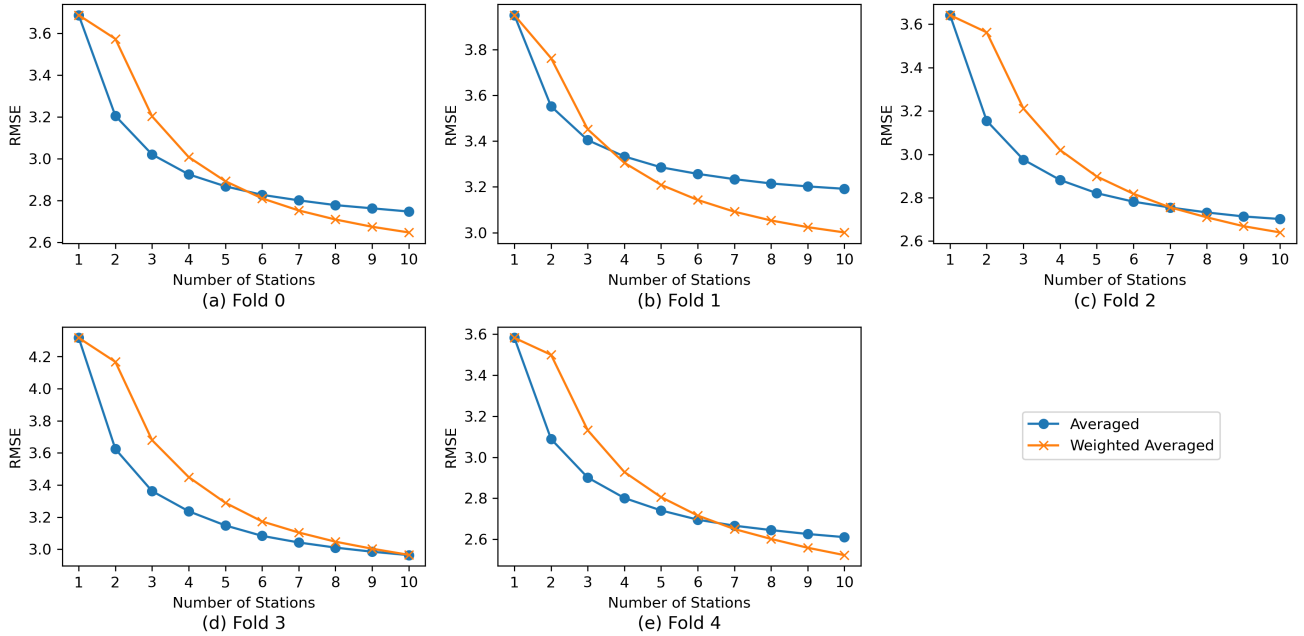


Fig. 7. RMSE of Averaged and Weighted Averaged Models with 1–10 Available Stations Obtained from Year 2018 Testing Datasets.

increases the true positive rate along with the false discovery rate. The number of stations selected from the ensemble methods should be considering the balance between the event capture rate and number of false positives.

Generally, the weighted averaged method demonstrates a higher accuracy and event detection rate compared the averaged method. However, for both methods the true positive rate decreases as the number of stations increases. This phenomenon is due to the low accuracy of the weak predictors and the smoothing effect of the averaging methods. The averaging methods are filtering out the lower extremes of the prediction results. Therefore, a third method or the weighted voting method is proposed. The weighted voting method collects a weighted vote from each of the weak predictors and aggregates the votes. The vote positive when the prediction result is smaller than the triggering temperature zero degrees, else the vote is negative. The weights are computed by the same algorithm of the weighted averaged models.

Figures 6 and 8 compared the true positive rate and false discovery rate of the weighted voting method with the previous two methods. The true positive rates have significantly increased compared to the previous methods, when utilizing the same number of stations. However, the false discovery rate also increased. To further increase the true positive rate without the increase of false discovery rate of the spatial interpolation-based methods, the accuracy of the weak predictor models should be further improved.

#### D. Limitations and Open Challenges

After testing the proposed method with the baseline, there are a few limitations of the method detected. These limitations

are open challenges that lead toward future development of spatial interpolation-based frost prediction methods.

1) *Further improvement of the accuracy*: The errors of the proposed method are higher than the baseline created from on-site datasets. High event capture rates of the proposed method are only achieved with high numbers of false positives. To decouple event capture rate with the number of false positives, the increase of accuracy is inevitable. With the current accuracy, spatial interpolation-based methods cannot fully replace previous methods based on on-site historical datasets and sensors.

2) *Lacking of ground truth to validate models*: As spatial interpolation-based models are constructed with five-fold validation, the testing datasets are limited [21]. In this article, the testing datasets are generated from 15 weather stations for each fold. Therefore, any accuracy metrics can only represent the accuracy on these 15 weather stations. In the production environment, predictions are required on other locations. The model accuracy on other locations is uncertain. In future works, more weather stations could be involved to reduce this uncertainty.

3) *Models are highly sensitive to the choice of training weather stations*: As shown by experiment 1, raster maps produced from models of different folds are significantly different from each other. The models are affected by choices of training weather stations. From experiment 2, this choice also affects the accuracy of models. In future model construction with cross-validation, the accuracy of each fold should be carefully examined. A possible method to mitigate this issue is the increase in the number of weather stations. As the number of stations increases, the effect of individual stations reduces.



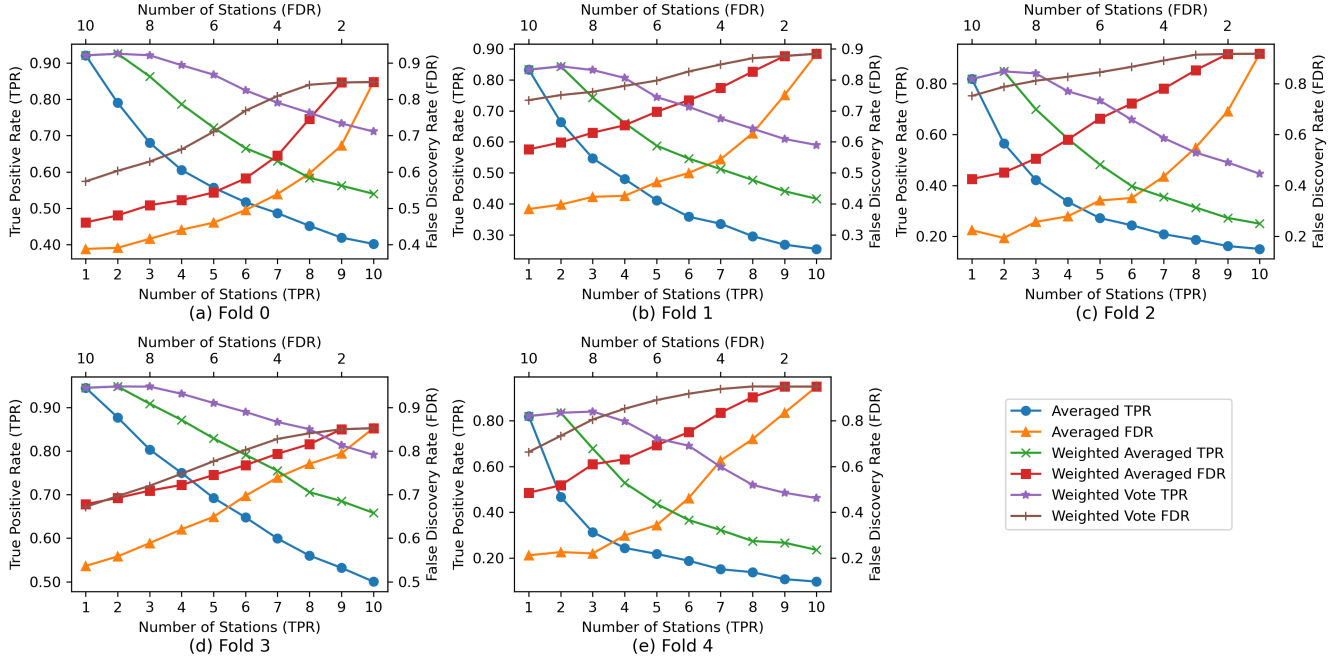


Fig. 8. True Positive Rate and False Discovery Rate of Averaged, Weighted Averaged, and Weighted Voting Models with 1–10 Available Stations Obtained from Year 2018 Testing Datasets.

4) *Application of similar methods to other domains:* The recent frost prediction methods mentioned in Section I all predicts the local condition with local historical climate data-based models. Data availability is an inevitable factor to consider when constructing these models. Some other domains using local historical data could also be impacted by data availability. Therefore, these domains could also benefit from the proposed method in this article. Domains such as forest fire forecasting [22] and soil property prediction [23] that are evolving with spatial methods could be further explored with a varied version of the proposed method. Other fields such as rain forecasting and atmospheric weather forecasting [24] could implement the proposed method as an exploration of a fault-tolerance design.

#### IV. CONCLUSION

This article proposes a spatial interpolation-based frost prediction method. This method aims to eliminate the dependency of on-site historical datasets/sensors during model training, validation, testing, and future operations. The climate data is from weather stations in the NSW and ACT areas of Australia. Climate data from 75 weather stations are obtained. DEM and NDVI datasets of the study area are also utilized. The proposed methods are ensemble learning methods based on ANN models. The two ensemble methods are averaging and weighted averaging of weak predictors. Each weak predictor is constructed using one weather station as the climate data source. These models are also constructed with five-fold validation with the weather station data divided into five testing data folds. For each testing data fold, the other weather stations are used as training data sources. The baseline models

are ANN models trained with on-site historical data. There are three experiments conducted to test the performance of models. The first experiment compares the raster map outputs of spatial interpolation-based models. Raster maps are constructed from the individual weak predictors, averaged results of weak predictors, and weighted averaged results of weak predictors. The results of the T-tests show that the raster maps for different folds are significantly different from each other. This shows that the models are significantly affected by the training datasets, hence, the division of folds is important. The second experiment shows that the weighted averaged method provides the lowest error among the spatial interpolation-based methods. After that, the final experiment reveals the effect of the number of available stations. Accuracy increases as the number of available stations increases. However, the event capture rate increases with the reduction of station number. This increase is related to the increase of false positives. Apparently, higher errors induce the triggering of more events, which increases both event capture rate and false positives. The experiments indicate three limitations of the work. The first limitation is accuracy. Accuracy needs to be increased to eliminate the relationship between high event capture rate and high false positives. Also, as a spatial interpolation-based method constructed by five-fold validation, only 15 stations per fold act as the ground truth to test the models. Finally, the models are highly sensitive to the choice of training weather stations. This uncovers the importance of fold selection. In conclusion, the proposed spatial interpolation-based frost prediction method could capture frost events and be deployed as an alternative when on-site historical datasets are temporarily unavailable.

APPENDIX A  
 RASTER MAPS GENERATED FROM MODELS CREATED BY  
 DIFFERENT WEATHER STATIONS

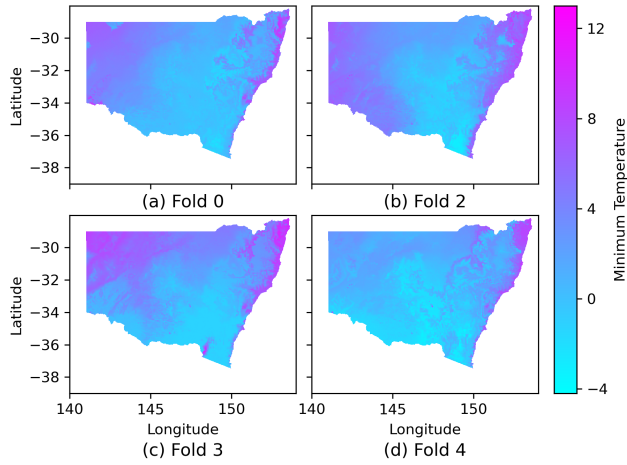


Fig. 9. Raster Maps from Models Using Weather Station 66137 as Climate Data Source Trained with the Datasets from Folds 0, 2, 3, and 4.

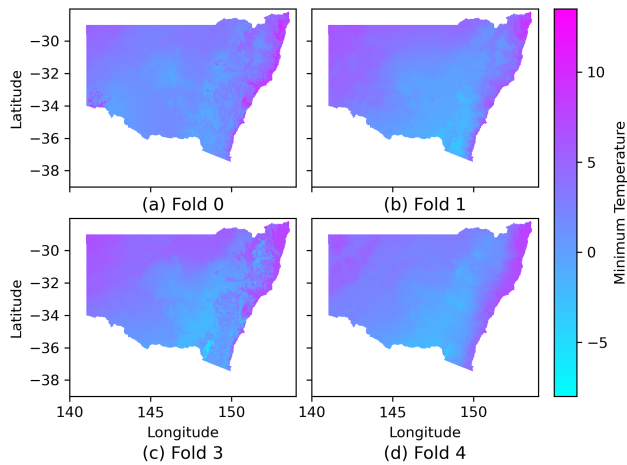


Fig. 10. Raster Maps from Models Using Weather Station 58212 as Climate Data Source Trained with the Datasets from Folds 0, 1, 3, and 4.

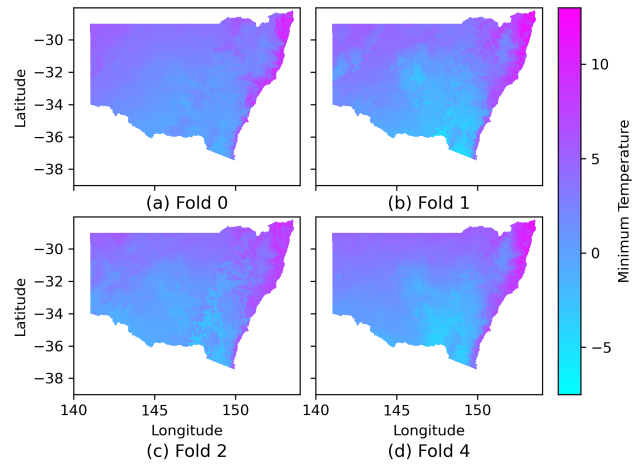


Fig. 11. Raster Maps from Models Using Weather Station 72160 as Climate Data Source Trained with the Datasets from Folds 0, 1, 2, and 4.

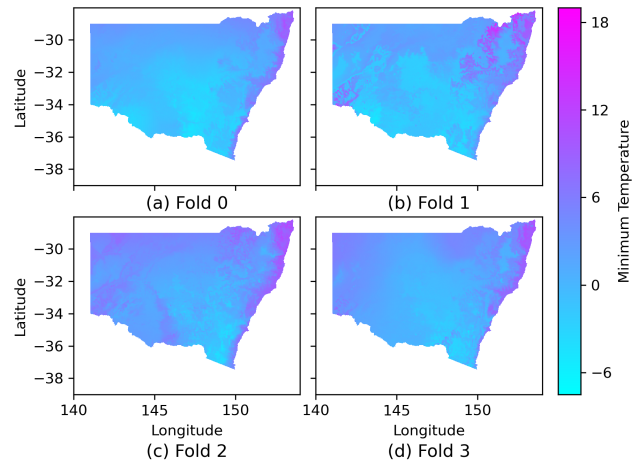


Fig. 12. Raster Maps from Models Using Weather Station 67119 as Climate Data Source Trained with the Datasets from Folds 0–3.

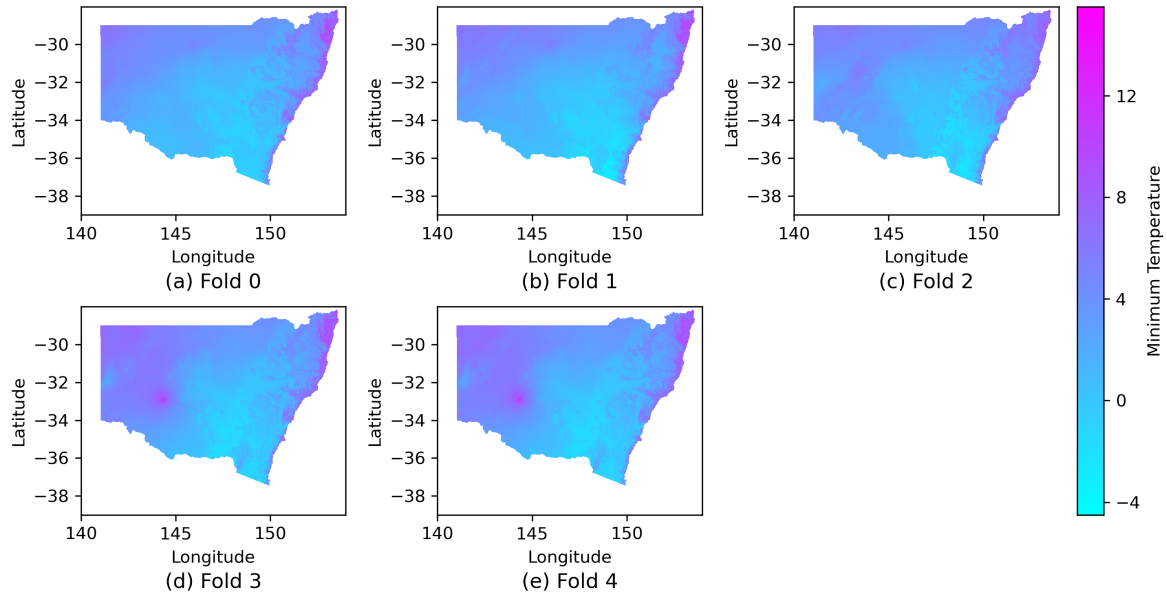


Fig. 13. Raster Maps from Weighted Averaged Results per Fold.

APPENDIX B

P-VALUE MATRICES COMPARING RASTER MAP RESULTS GENERATED FROM DIFFERENT FOLDS

TABLE V

P-VALUE MATRIX FOR COMPARING RASTER MAP RESULTS OF MODELS USING WEATHER STATION 66137 AS CLIMATE DATA SOURCE AND TRAINED WITH THE DATASETS FROM FOLDS 0, 2, 3, 4

	Fold 0	Fold 2	Fold 3	Fold 4
Fold 0	N/A	0.00	0.00	0.00
Fold 2	0.00	N/A	0.00	0.00
Fold 3	0.00	0.00	N/A	0.00
Fold 4	0.00	0.00	0.00	N/A

TABLE VI

P-VALUE MATRIX FOR COMPARING RASTER MAP RESULTS OF MODELS USING WEATHER STATION 58212 AS CLIMATE DATA SOURCE AND TRAINED WITH THE DATASETS FROM FOLDS 0, 1, 3, 4

	Fold 0	Fold 1	Fold 3	Fold 4
Fold 0	N/A	8.83e-206	0.00	0.00
Fold 1	8.83e-206	N/A	0.00	0.00
Fold 3	0.00	0.00	N/A	0.00
Fold 4	0.00	0.00	0.00	N/A

TABLE VII

P-VALUE MATRIX FOR COMPARING RASTER MAP RESULTS OF MODELS USING WEATHER STATION 72160 AS CLIMATE DATA SOURCE AND TRAINED WITH THE DATASETS FROM FOLDS 0, 1, 2, 4

	Fold 0	Fold 1	Fold 2	Fold 4
Fold 0	N/A	0.00	0.00	0.00
Fold 1	0.00	N/A	0.00	6.91e-22
Fold 2	0.00	0.00	N/A	0.00
Fold 4	0.00	6.91e-22	0.00	N/A

TABLE VIII

P-VALUE MATRIX FOR COMPARING RASTER MAP RESULTS OF MODELS USING WEATHER STATION 67119 AS CLIMATE DATA SOURCE AND TRAINED WITH THE DATASETS FROM FOLDS 0-3

	Fold 0	Fold 1	Fold 2	Fold 3
Fold 0	N/A	0.00	0.00	0.00
Fold 1	0.00	N/A	0.00	0.00
Fold 2	0.00	0.00	N/A	0.00
Fold 3	0.00	0.00	0.00	N/A

TABLE IX

P-VALUE MATRIX FOR COMPARING WEIGHTED AVERAGED RASTER MAP RESULTS OF EACH FOLD

	Fold 0	Fold 1	Fold 2	Fold 3	Fold 4
Fold 0	N/A	0.00	0.00	0.00	0.00
Fold 1	0.00	N/A	0.00	0.00	0.00
Fold 2	0.00	0.00	N/A	0.00	0.00
Fold 3	0.00	0.00	0.00	N/A	0.00
Fold 4	0.00	0.00	0.00	0.00	N/A

APPENDIX C  
WEATHER STATION LOCATION COORDINATES

TABLE X  
WEATHER STATION LOCATION COORDINATES

Station ID	Latitude (Degrees)	Longitude (Degrees)	Fold Number
70351	-35.3088	149.2004	0
70217	-36.2939	148.9725	0
65103	-33.3627	147.9205	0
66194	-33.9057	151.1134	0
68192	-34.0390	150.6890	0
75041	-34.2487	146.0695	0
66037	-33.9465	151.1731	0
63291	-33.4119	149.6540	0
73138	-34.2493	148.2475	0
51049	-31.9861	147.9489	0
62100	-32.7244	150.2290	0
58198	-28.8353	153.5585	0
67113	-33.7195	150.6783	0
61078	-32.7939	151.8364	0
61363	-32.0335	150.8264	0
69148	-35.9004	150.1437	1
61287	-32.1852	150.1737	1
51161	-30.9776	148.3798	1
74148	-34.7050	146.5140	1
58208	-28.8824	153.0618	1
66161	-33.9925	150.9489	1
62101	-32.5628	149.6149	1
47048	-32.0012	141.4694	1
65068	-33.1281	148.2428	1
69139	-36.6722	149.8191	1
59007	-31.0711	152.7717	1
58214	-28.8305	153.2601	1
60141	-31.8895	152.5120	1
68262	-34.3335	150.2670	1
66137	-33.9176	150.9837	1
58012	-29.4325	153.3632	2
75019	-34.5412	144.8345	2
56238	-30.5273	151.6158	2
63292	-33.6185	150.2741	2
49000	-32.8833	144.3092	2
67105	-33.6004	150.7761	2
63303	-33.3768	149.1263	2
58077	-29.6224	152.9605	2

TABLE XI  
WEATHER STATION LOCATION COORDINATES (CONT.)

Station ID	Latitude (Degrees)	Longitude (Degrees)	Fold Number
68257	-34.0615	150.7735	2
66212	-33.8338	151.0718	2
55202	-30.9537	150.2494	2
68242	-34.6532	150.8609	2
74258	-35.5575	144.9458	2
65111	-33.8382	148.6540	2
58212	-29.1830	153.3964	2
70330	-34.8085	149.7311	3
48245	-30.0362	145.9521	3
54038	-30.3154	149.8302	3
72160	-36.0690	146.9509	3
72162	-36.2304	148.1405	3
72161	-35.9371	148.3779	3
50017	-33.9382	147.1962	3
60139	-31.4335	152.8655	3
61375	-33.2894	151.2107	3
68072	-34.9469	150.5353	3
68239	-34.5253	150.4217	3
61425	-33.4351	151.3614	3
46012	-31.5194	143.3850	3
64017	-31.3330	149.2699	3
69128	-35.1103	150.0826	3
68228	-34.3691	150.9291	4
67108	-33.8969	150.7281	4
69137	-37.2622	150.0504	4
52088	-30.0372	148.1223	4
61392	-31.7416	150.7937	4
67119	-33.8510	150.8567	4
55325	-31.0742	150.8362	4
61055	-32.9184	151.7985	4
50137	-33.0682	147.2133	4
69138	-35.3635	150.4828	4
61366	-33.2814	151.5766	4
65070	-32.2206	148.5753	4
61260	-32.7886	151.3377	4
69147	-36.9077	149.8989	4
68241	-34.5638	150.7900	4

ACKNOWLEDGMENT

We would like to acknowledge the support of Food Agility CRC Ltd, 81 Broadway, Ultimo, NSW, 2007, Australia, funded under the Commonwealth Government CRC Program. The CRC Program supports industry-led collaborations between industry, researchers and the community.

REFERENCES

[1] Q. Ma, J.-G. Huang, H. Hänninen, and F. Berninger, "Divergent trends in the risk of spring frost damage to trees in Europe with recent warming," *Global Change Biology*, vol. 25, no. 1, pp. 351–360, Oct. 2019.

[2] R. L. Snyder and J. d. Melo-Abreu, "Economic importance of frost damage," in *Frost protection: fundamentals, practice and economics*. FAO, 2005, vol. 1, ch. 1, sec. 7, pp. 11–12.

- [3] I. Zhou, J. Lipman, M. Abolhasan, N. Shariati, and D. W. Lamb, "Frost monitoring cyber-physical system: A survey on prediction and active protection methods," *IEEE Internet of Things Journal*, vol. 7, no. 7, pp. 6514–6527, Jul. 2020.
- [4] J. Li and A. D. Heap, "Spatial interpolation methods applied in the environmental sciences: A review," *Environmental Modelling & Software*, vol. 53, pp. 173–189, 2014. [Online]. Available: <https://www.sciencedirect.com/science/article/pii/S1364815213003113>
- [5] T. Appelhans, E. Mwangomo, D. R. Hardy, A. Hemp, and T. Nauss, "Evaluating machine learning approaches for the interpolation of monthly air temperature at Mt. Kilimanjaro, Tanzania," *Spatial Statistics*, vol. 14, pp. 91–113, 2015, spatial and Spatio-Temporal Models for Interpolating Climatic and Meteorological Data. [Online]. Available: <https://www.sciencedirect.com/science/article/pii/S2211675315000482>
- [6] T. N. Carlson and D. A. Ripley, "On the relation between NDVI, fractional vegetation cover, and leaf area index," *Remote Sensing of Environment*, vol. 62, no. 3, pp. 241–252, 1997. [Online]. Available: <https://www.sciencedirect.com/science/article/pii/S0034425797001041>
- [7] D. di Francescantonio, M. Villagra, G. Goldstein, and P. I. Campanello, "Drought and frost resistance vary between evergreen and deciduous Atlantic Forest canopy trees," *Functional Plant Biology*, Jun. 2020.
- [8] V. Halley, M. Eriksson, and M. Nunez, "Frost prevention and prediction of temperatures and cooling rates using GIS," *Australian Geographical Studies*, vol. 41, no. 3, pp. 287–302, Nov. 2003.
- [9] L. E. Iacono, J. L. Vázquez Poletti, C. García Garino, and I. M. Llorente, "Performance models for frost prediction in public cloud infrastructures," *Computing and Informatics*, vol. 37, no. 4, pp. 815–837, 2018.
- [10] A. L. Diedrichs, F. Bromberg, D. Dujovne, K. Brun-Laguna, and T. Watteyne, "Prediction of frost events using machine learning and IoT sensing devices," *IEEE Internet of Things Journal*, vol. 5, no. 6, pp. 4589–4597, Dec. 2018.
- [11] L. Ghielmi and E. Eccel, "Descriptive models and artificial neural networks for spring frost prediction in an agricultural mountain area," *Computers and Electronics in Agriculture*, vol. 54, no. 2, pp. 101–114, Dec. 2006.
- [12] W. Zeng, Z. Zhang, and C. Gao, "A Levenberg-Marquardt neural network model with rough set for protecting citrus from frost damage," in *Proc. 2012 Eighth International Conference on Semantics, Knowledge and Grids*, Beijing, China, Oct. 2012, pp. 193–196.
- [13] M. Fuentes, C. Campos, and S. García-Loyola, "Application of artificial neural networks to frost detection in central Chile using the next day minimum air temperature forecast," *Chilean journal of agricultural research*, vol. 78, no. 3, pp. 327–338, 2018.
- [14] Bureau of Meteorology. (2021) Weather Station Directory. Bureau of Meteorology. [Accessed: April 04, 2021]. [Online]. Available: <http://www.bom.gov.au/climate/data/stations/>
- [15] —. (2018) Australia in winter 2018. Bureau of Meteorology. [Accessed: April 04, 2021]. [Online]. Available: <http://www.bom.gov.au/climate/current/season/aus/archive/201808.summary.shtml>
- [16] J. Gallant, N. Wilson, T. Dowling, A. Read, and C. Inskeep. (2011) SRTM-derived 1 Second Digital Elevation Models Version 1.0. Geoscience Australia. [Accessed: April 04, 2021]. [Online]. Available: <http://pid.geoscience.gov.au/dataset/ga/72759>
- [17] K. Didan. (2021) MOD13Q1 MODIS/Terra Vegetation Indices 16-Day L3 Global 250m SIN Grid V006. NASA EOSDIS Land Processes DAAC. [Accessed: April 04, 2021]. [Online]. Available: <https://doi.org/10.5067/MODIS/MOD13Q1.006>
- [18] Department of Industry, Science, Energy and Resources. (2020) NSW State Boundary - Geoscape Administrative Boundaries. Department of Industry, Science, Energy and Resources. [Accessed: April 04, 2021]. [Online]. Available: <https://data.gov.au/data/dataset/a1b278b1-59ef-4dea-8468-50eb09967f18>
- [19] —. (2020) ACT State Boundary - Geoscape Administrative Boundaries. Department of Industry, Science, Energy and Resources. [Accessed: April 04, 2021]. [Online]. Available: <https://data.gov.au/data/dataset/83468f0c-313d-4354-9592-289554eb2dc9>
- [20] M. Lee, S. Moon, Y. Kim, and B. Moon, "Correcting abnormalities in meteorological data by machine learning," in *2014 IEEE International Conference on Systems, Man, and Cybernetics (SMC)*, San Diego, CA, USA, 2014, pp. 888–893.
- [21] D. R. Roberts, V. Bahn, S. Ciuti, M. S. Boyce, J. Elith, G. Guillera-Arroita, S. Hauenstein, J. J. Lahoz-Monfort, B. Schröder, W. Thuiller, D. I. Warton, B. A. Wintle, F. Hartig, and C. F. Dormann, "Cross-validation strategies for data with temporal, spatial, hierarchical, or phylogenetic structure," *Ecography*, vol. 40, no. 8, pp. 913–929, 2017. [Online]. Available: <https://onlinelibrary.wiley.com/doi/abs/10.1111/ecog.02881>
- [22] O. Ghorbanzadeh, K. Valizadeh Kamran, T. Blaschke, J. Aryal, A. Naboureh, J. Eimali, and J. Bian, "Spatial prediction of wildfire susceptibility using field survey gps data and machine learning approaches," *Fire*, vol. 2, no. 3, 2019. [Online]. Available: <https://www.mdpi.com/2571-6255/2/3/43>
- [23] P. Ryan, N. McKenzie, D. O'Connell, A. Loughhead, P. Leppert, D. Jacquier, and L. Ashton, "Integrating forest soils information across scales: spatial prediction of soil properties under australian forests," *Forest Ecology and Management*, vol. 138, no. 1, pp. 139–157, 2000. [Online]. Available: <https://www.sciencedirect.com/science/article/pii/S0378112700003935>
- [24] N. L. and M. H.S., "Atmospheric weather prediction using various machine learning techniques: A survey," in *2019 3rd International Conference on Computing Methodologies and Communication (ICCMC)*, 2019, pp. 422–428.